Seismic analysis of motorway bridges accounting for key structural components and nonlinear soil-structure interaction

Anastasopoulos, Ioannis; Sakellariadis, L.; Agalianos, A.

Published in:
Soil Dynamics and Earthquake Engineering

DOI:
10.1016/j.soildyn.2015.06.016

Publication date:
2015

Document Version
Peer reviewed version

Seismic analysis of motorway bridges accounting for key structural components and nonlinear soil–structure interaction

by

I. Anastasopoulos[1], L. Sakellariadis[2] and A. Agalianos[3]

Abstract

The paper introduces an efficient methodology to analyze the seismic performance of motorway bridges. Rigorous 3D models of a typical overpass bridge are developed and used to assess the efficiency of the proposed method. Fixed-base conditions are initially considered to focus on the effect of key structural components. The proposed simplified model is composed of a SDOF system of a pier with lateral and rotational springs and dashpots connected at the top, representing the deck and the abutment bearings. Its definition requires section analysis of the pier, and computation of spring and dashpot coefficients using simple formulas. It is shown that the lateral and rotational restraint provided by the deck and the abutment bearings is not at all negligible and should be taken into account. The simplified model is extended to account for nonlinear soil–structure interaction, replacing the soil–foundation system with horizontal, vertical, and rotational springs and dashpots. While the horizontal and vertical springs and dashpots are assumed elastic, the nonlinear rotational spring is defined on the basis of non–dimensional moment–rotation relations. The simplified model compares well with the full 3D model of the bridge–abutment–foundation–soil system, and is therefore considered a reasonable approximation.

[1] Professor, Division of Civil Engineering, University of Dundee; formerly National Technical University of Athens
[2] Civil Engineer, MSc, University of Dundee; formerly National Technical University of Athens
[3] Civil Engineer, MSc, University of Dundee; formerly National Technical University of Athens

Keywords

Seismic vulnerability; bridge pier; nonlinear analysis; soil-structure interaction;

1. Introduction

Motorway networks are indispensable for day-to-day life in modern societies. They are typically composed of various components, including bridges, tunnels, and embankments. Bridges are generally acknowledged to be the most vulnerable. Their severe damage or collapse, such as that of the Fukae section (**Fig. 1a**) during the 1995 Kobe earthquake [Kawashima & Unjoh, 1997], may pose a severe threat to the motorists (**Fig. 1b**). Even if the main shock doesn't lead to collapse, a severely damaged bridge may be unsafe during subsequent aftershocks [Franchin & Pinto, 2009]. In such a case, emergency inspection is necessary and preventive closure of the motorway may be the only safe option. However, such an action will unavoidably lead to obstruction of rescue operations, and may inflict severe indirect losses. Hence, there is an urgent need for development and implementation of emergency response systems for motorway networks.

A variety of emergency response systems have been developed so far, including global earthquake management systems [GDACS, www.gdacs.org, De Groeve et al., 2006; WAPMERR, www.wapmerr.org; Erdik et al., 2011], and local systems for real-time damage assessment at the city level [Erdik et al., 2003]. In the case of transportation systems, there have been some first attempts [e.g., Codermatz et al., 2003], but to the best of our knowledge, there are no well documented emergency response systems for motorway networks. Such a RApid REsponse (RARE) system is currently being developed, using the Attiki Odos Motorway (Athens, Greece) as a case study. As discussed in Anastasopoulos et

al. [2014], the development of such a RARE system requires: (a) a comprehensive GIS database of the motorway, including the locations and typologies of the various structures; (b) a network of accelerographs to record the seismic motions at characteristic locations along the motorway; and (c) a real-time damage assessment method.

Such a method has been outlined in Anastasopoulos et al. [2014], combining finite element (FE) simulations with advanced statistical modeling. For each bridge type, the method requires: (i) nonlinear dynamic time history analyses with an adequately large number of seismic excitations; (ii) development of a dataset of the seismic damage, expressed by appropriate damage indices (DIs), as a function of the seismic excitation, expressed by a variety of intensity measures (IMs); and (iii) development of a nonlinear regression model, expressing the seismic damage (using one or more DIs) as a function of a number of statistically significant IMs. In contrast to previous research, which aimed at identifying efficient IMs [e.g., Housner, 1952; Arias, 1970], the proposed method develops nonlinear regression models, combining an optimum number of statistically significant IMs.

Previous studies have shown that a single IM is not always adequate to capture all of the characteristics of a seismic motion [e.g., Garini & Gazetas, 2013]. In Anastasopoulos et al. [2014], this was demonstrated using an idealized (single) bridge pier as an illustrative example. One such example is shown in **Fig. 2a**, referring to the correlation of the maximum drift ratio $\delta_{r,max}$ (a typical DI):

$$\delta_{r,max} = \frac{\delta_{max}}{h} * 100\% \quad (1)$$

with one of the most efficient IMs, the Velocity Spectrum Intensity, *VSI* [Von Thun et al., 1988]. It is worth observing that for *VSI* = 3 m, the maximum drift ratio $\delta_{r,max}$ varies from less than 1 (minor damage) to more than 3 (severe damage or collapse).

An example of the efficiency of the nonlinear regression equations [Anastasopoulos et al., 2014] is depicted in **Fig. 2b**, which compares the observed $\delta_{r,max}$ to the predicted value, according to the equation:

$$\delta_{r,\max} = \mathrm{EXP}\left[\begin{array}{c} 0.70612*\mathrm{LN(PGA)} + 12.97257*\frac{1}{\mathrm{PGV}} - 2.50142*\frac{1}{\sqrt{\mathrm{PGD}}} - 3.18861*{A_{RMS}}^2 + \\ +1.46808*\frac{1}{\sqrt{D_{RMS}}} - 0.18791*\frac{1}{\sqrt{I_C}} - 11.8121*\frac{1}{\sqrt{S_E}} + 212.77053*\frac{1}{\mathrm{CAV}} + \\ +0.10551*\sqrt{\mathrm{VSI}} - 0.04486*\sqrt{H_I} - 0.02203*\frac{1}{\mathrm{SMA}} + 3.05564*\frac{1}{\mathrm{SMV}} + \\ +0.1741*\mathrm{LN}(T_P) - 0.28233*\frac{1}{\mathrm{T}_{mean}} + 0.18476*\sqrt{D_{sig}} \end{array}\right] \quad (2)$$

where *PGA*, *PGV*, and *PGD*: peak ground acceleration, velocity, and displacement; A_{RMS} and D_{RMS}: RMS acceleration and displacement; *IC*: characteristic intensity; S_E: specific energy density; *CAV*: cumulative absolute velocity; H_I: Housner intensity; *SMA* and *SMV* sustained maximum acceleration and velocity; T_P and T_{mean}: predominant and mean period; and D_{sig} : significant duration. The efficiency of the equation is expressed additionally in terms of Adjusted R-squared (R^2), average deviation, and mean absolute percentage error (MAPE):

$$MAPE = \frac{1}{n}\sum_{i=1}^{n}|PE_i| \quad (3)$$

where $PE_i = 100\%\left(Y_i - \widehat{Y}_i\right)/Y_i$ is the percentage error for observation *i* of the actual damage index value *Y*, and the model-estimated damage index value $\widehat{Y}_i$, for observation. From such results, it can be concluded that the nonlinear regression model equations reduce significantly the deviations between the predicted and the observed results.

Such equations are easily programmable and can be employed for real-time damage assessment. As sketched in **Fig. 3**, in the event of an earthquake the real-time system will record seismic accelerations at various locations along the motorway. This way, the seismic motion will be available in real time, right after the occurrence of the earthquake. For each bridge (or other kind of structure), the nearest record(s) will be used to assess the seismic damage employing the developed equations. Such knowledge of the seismic excitation is a

major difference to traditional risk assessment, in which case the seismic excitation cannot possibly be predicted, and hence probabilistic approaches are much more appropriate.

Still though, developing such equations for all the bridges of a motorway requires quite substantial computational effort. For example, for the idealized bridge pier that was analyzed in Anastasopoulos et al. [2014], about 350 nonlinear dynamic time history analyses were required to generate a statistically significant dataset. Such an effort would be much more arduous if an actual bridge system was analyzed, and would not be easily implementable at the level of an entire motorway which typically includes a few hundreds of bridges. Hence, in order to implement a RARE system, there is a need to develop adequately simplified models of typical motorway bridges. The key objective of the present paper is to develop an efficient analysis methodology, taking account of the key components of the structural system of the bridge (deck, abutment bearings), as well as the effect of soil–structure interaction (SSI).

2. Bridge typologies of the Attiki Odos motorway

A variety of bridge typologies can be found around the world, rendering the task of developing a global classification rather ambitious. The present study focuses on modern motorway bridges, such as those encountered in the newly built Attiki Odos motorway in Athens, Greece. The latter is used as a case study for a RARE system that is currently being developed, and is therefore of particular interest. With a total length of 65 km, Attiki Odos is a modern motorway serving as a ring road of the greater metropolitan area of Athens. It includes a variety of critical structures, such as bridges, tunnels, retaining walls, slopes, and embankments. A total of 192 bridges can be found along the motorway, including 29 interchanges (**Fig. 4a**), and 163 overpass or underpass (road or rail) bridges (**Fig. 4b**).

With such a large number of motorway bridges, there is a need for classification in representative classes. Such a classification is performed herein following the corresponding classification schemes of ATC-13 [1985], NBI [FHWA 1995], HAZUS [FEMA-NIBS 2004], and the work of Argyroudis et al. [2003], Nielson & DesRoches [2007], and Moschonas et al. [2009]. A comprehensive review of the state of the art on the subject can be found in Pitilakis et al. [2014] and Pitilakis & Crowley [2014]. More specifically, the following parameters are considered: (a) the number of spans; (b) the type of the deck (continuous or simply supported); and (c) the type of the pier-to-deck connection (fixed, bearings, or combination). Based on these criteria, the 192 bridges of the Attiki Odos motorway can be classified as summarized in **Table 1** and **Fig. 5**.

3. Problem definition and analysis methodology

A typical overpass bridge (A01-TE20) of the Attiki Odos Motorway, belonging to the MSCF/B class, is selected as an illustrative example. Besides its simplicity, the selected bridge system is representative for about 30% of the bridges of the specific motorway, and is also considered quite common for metropolitan motorways in general. As shown in **Fig. 6a**, the selected system is a symmetric 3-span bridge with a continuous pre-stressed concrete box-girder deck, supported on two reinforced concrete (RC) cylindrical piers of diameter d = 2 m and height h = 8.8 m. The piers are monolithically connected to the deck, which is supported by 4 elastomeric bearings at each abutment. Each bearing is 0.3 m x 0.5 m (longitudinal x transverse) in plan and has an elastomer height t = 63 mm. The piers are founded on B = 8 m square footings, while the abutments consist of retaining walls of 9 m height and 1.5 m thickness. The latter are connected to two side walls of 0.6 m thickness and founded on a rectangular 7 m x 10.4 m rectangular footing.

The seismic performance of the bridge is analyzed employing the FE method. Two detailed models are developed for this purpose: (a) a simpler 3D model assuming fixed base conditions (**Fig. 6b**); and (b) a more rigorous 3D model, taking account of the foundations, the abutments, and the soil (**Fig. 6c**). In both cases, the deck and the piers are modeled with elastic and inelastic beam elements, respectively. The reinforcement of the d = 2 m RC piers has been computed according to the provisions of the Greek Code for Reinforced Concrete (ΕΚΩΣ, 2000) for columns with large ductility demands. The inelastic behavior of the piers is simulated with a nonlinear model, calibrated against the results of RC section analysis using the USC_RC software [2001]. The result of such a calibration is shown in **Fig. 6b**.

Linear elastic springs and dashpots are used to model the compression ($K_{c,b}$) and shear stiffness ($K_{s,b}$) and damping ($C_{c,b}$, $C_{s,b}$) of the bearings [e.g., Koh & Kelly, 1988]:

$$K_{c,b} = \frac{E_c\, A}{t\, n} \tag{4}$$

$$K_{s,b} = \frac{G\, A}{t\, n} \tag{5}$$

$$C_{c,b} = \frac{2\, K_{c,b}\, \xi}{\omega} \tag{6}$$

$$C_{s,b} = \frac{2\, K_{s,b}\, \xi}{\omega} \tag{7}$$

where E_c: the compression modulus of the elastomer; A: the plan area of the bearing; t: the thickness of the individual elastomer layers; n: the number of individual elastomer layers; G: the shear modulus of the elastomer; ξ: the damping coefficient of the bearing; and ω: the angular frequency of reference (assumed to be equal to the dominant mode of the bridge).

In the case of the full 3D model of the bridge–foundation–abutment–soil system (**Fig. 6c**), the footings and the abutments are modeled with elastic hexahedral continuum elements, assuming the properties of RC (E = 30 GPa). An idealized 20 m deep substratum of homogeneous stiff clay is considered, having undrained shear strength S_u = 150 kPa. The

latter is also modeled with hexahedral continuum elements. Nonlinear soil behavior is modeled with a kinematic hardening model, with a Von Mises failure criterion and associated flow rule [Anastasopoulos et al., 2011]. The evolution law of the model consists of a nonlinear kinematic hardening component, which describes the translation of the yield surface in the stress space, and an isotropic hardening component, which defines the size of the yield surface as a function of plastic deformation [Gerolymos & Gazetas, 2005]. Calibration of model parameters requires knowledge of: (a) the undrained shear strength S_u ; (b) the small–strain stiffness (expressed through G_o or V_s); and (c) the stiffness degradation (G–γ and ξ–γ curves). More details on the model can be found in Anastasopoulos et al. [2011].

Appropriate *"free–field"* boundaries are used at the lateral boundaries of the model, while dashpots are installed at the base of the model to simulate the half-space underneath the 20 m of the soil that is included in the 3D model. Special contact elements are introduced at the soil–footing interfaces to model possible separation (uplifting) and sliding. A friction coefficient μ = 0.7 is assumed, which is considered realistic for the soil conditions investigated herein. The same applies to the interfaces between the abutment and the embankment soil. A reinforced soil embankment is considered, which is quite common in such motorway bridges (due to space limitations). The latter is modeled in a simple manner, by installing appropriate kinematic constraints in the transverse direction.

4. Simplified models for fixed–base conditions

The previously described detailed models of the bridge (**Fig. 6**) are used as reference in order to test the efficiency of the proposed simplified models. Initially, SSI is ignored to focus on the effect of the structural components of the bridge (deck and abutment

bearings). In the next section, the simplified models are extended to account for nonlinear SSI. The predictions of the simplified models are compared to the detailed model of the bridge, assuming fixed–base conditions (**Fig. 6b**). The comparison is performed in terms of static and dynamic loading. In the first case, the models are subjected to monotonic pushover loading, while dynamic time history analyses are performed for the latter. For this purpose, 29 real seismic records are used as seismic excitation, carefully chosen to cover a wide range of excitation characteristics (**Fig. 7**). The seismic performance is compared in terms of maximum ($\delta_{r,max}$) and residual ($\delta_{r,res}$) drift ratio, and with respect to the ratio of ductility demand over ductility capacity (μ_d/μ_c).

Transverse direction

The response of a bridge in the transverse direction is usually considered straight–forward and a SDOF system is a typical, very common, approximation. While for long multi–span bridges this may be acceptable, for the cases examined herein it may lead to gross errors if the contribution of the deck and of the abutment bearings are not taken into account. To illustrate the effect of each structural component, three simplified systems (**Fig. 8**) are developed and comparatively assessed.

The first one (System A) considers an equivalent SDOF system of a single bridge pier, ignoring the contribution of the deck. As illustrated in **Fig. 8a**, the SDOF system is composed of a column having the stiffness, height, and moment–curvature (*M*–*c*) response of the pier and a concentrated mass m_p:

$$m_p = m_d \frac{K_p}{K_B} \tag{8}$$

where $K_p = 3EI_p/h^3$ (E, I_p, and h: the Young's modulus (RC), the moment of inertia, and the height of the pier, respectively) is the stiffness of the pier, and K_B is the stiffness of the entire bridge, taking account of the shear stiffness $K_{s,b}$ of the abutment bearings:

$$K_B = \sum K_{s,b} + \sum K_p \tag{9}$$

The second simplified model (System B) incorporates the shear stiffness of the abutment bearings. As depicted in **Fig. 8b**, a lateral spring ($K_{s,t}$) and a lateral dashpot ($C_{s,t}$) are added at the top of the SDOF system, being computed as follows:

$$K_{s,t} = \sum K_{s,b} \tag{10}$$

$$C_{s,t} = \frac{2\,K_{s,t}\,\xi_s}{\omega} \tag{11}$$

where ξ_s is the damping coefficient and ω the angular frequency of the bridge system. The mass of the deck is distributed as before.

The third and most complete simplified model (System C) also accounts for the rotational restraint that is provided by the deck. For this purpose, a rotational spring ($K_{r,t}$) and a rotational dashpot ($C_{r,t}$) are added at the top of the SDOF system, as depicted in in **Fig. 8c**. If the deck was rigidly connected to the abutments, the rotational stiffness would be equal to the torsional stiffness of the deck:

$$K_t = JG/L \tag{12}$$

where J is the torsion constant of the deck, L is the distance from the pier to the abutment, and G the shear modulus of the deck. In reality, however, the deck is connected to the abutment through the system of bearings, which has its own rotational compliance. Hence, the overall rotational stiffness is equal to that of the system of the two rotational springs in parallel:

$$K_{r,t} = \frac{K_t\,K_{r,b}}{K_t + K_{r,b}} \tag{13}$$

where $K_{r,b}$ is the rotational stiffness offered by the abutment bearings. Although the rotational stiffness of a single bearing is not significant, the rotational stiffness of the bearings acting as a system can be quite substantial. As sketched in **Fig. 8c**, the system of bearings resists the rotation of the deck by developing axial forces, and therefore $K_{r,b}$ can be computed as follows:

$$K_{r,b} = \sum K_{c,b} L^2 \tag{14}$$

where $K_{c,b}$ is the compressional stiffness of the bearings, and L the distance (in the transverse direction) of each bearing to the center of mass of the deck. As for System B, a rotational dashpot ($C_{r,t}$) is also added at the top of the SDOF system:

$$C_{r,t} = \frac{2\, K_{r,t}\, \xi_s}{\omega} \tag{15}$$

The performance of the three simplified models is comparatively assessed in **Fig. 9**, using as a benchmark the detailed 3D model of the bridge assuming fixed–base conditions (see **Fig. 6b**). The efficiency of the three simplified models is assessed on the basis of static pushover and dynamic time history analyses. In the first case, the monotonic pushover (F–δ) response of each simplified system is compared to the detailed bridge model (**Fig. 9a**). In the latter case, the results of all the dynamic time history analyses (for the 29 seismic excitations) are summarized in terms of predicted (according to the simplified models) vs. observed (detailed 3D model) ratio of ductility demand over ductility capacity μ_d/μ_c (**Fig. 9b**).

System A is proven unrealistically conservative, as it ignores the contribution of the lateral and rotational restraint that is provided by the deck and the system of abutment bearings. Observe that the pushover capacity predicted by System A is less than half of the capacity of the bridge, as computed using the detailed 3D model. The poor performance in terms of μ_d/μ_c of the dynamic time history analyses is therefore no surprise. As shown in

Fig. 9b, in 27% of the examined seismic excitations (8 out of 29) System A predicted total collapse of the bridge, in contrast to the results obtained with the detailed 3D model. Actually, in most of these cases, the bridge pier (according to the detailed 3D model) did not even exceed its ductility capacity ($\mu_d/\mu_c < 1$). Evidently, the contribution of the deck and of the abutment bearings is not at all negligible, and should be taken into account. This is an important finding, which denotes the inadequacy of over-simplified SDOF models.

This is only partially achieved with System B, which can be seen to perform better than System A, but cannot be considered as a reasonable approximation. The difference in terms of pushover capacity is smaller, but is still of the order of 40%. In terms of μ_d/μ_c, the differences are still quite substantial: the predicted μ_d/μ_c exceeds 2 in about 20% of the examined seismic excitations (6 out of 29), but at least total collapse is not erroneously predicted. Hence, accounting for the lateral stiffness of the abutment bearings leads to better results, but is not an acceptable approximation and the rotational restraint provided by the deck and the abutment bearings needs to be accounted for.

This is achieved with System C, the performance of which compares very well with that of the detailed 3D model of the bridge, both in terms of static pushover response and with respect to the dynamic time history analyses. The mean average percentage error (MAPE) is of the order of 10%. The same comparison has been performed for the maximum drift ratio $\delta_{r,\max}$ leading to the same qualitative conclusions [Agalianos & Sakellariadis, 2013]. Hence, System C is considered a reasonable approximation of the actual response of the bridge.

Longitudinal Direction

As illustrated in **Fig. 10**, three simplified models are introduced for the longitudinal direction. As for the transverse direction, the simpler one (System A) considers an equivalent SDOF system of a single bridge pier, assuming rotational fixity conditions at the top of the pier to account for the monolithically connected deck. This is a very common approximation for the longitudinal direction of such a bridge, based on the reasonable assumption that the flexural stiffness of the deck is much larger than that of the pier, and hence the rotation at the top of the pier is fully restrained. As depicted in **Fig. 10a**, the SDOF system is composed of a column having the stiffness, height, and moment–curvature (M–c) response of the pier and a concentrated mass m_p computed according to Eq. 8, but assuming $K_p = 12EI_p/h^3$ to account for the assumed full fixity conditions at the top of the pier.

As for the transverse direction, System B incorporates the shear stiffness of the abutment bearings. As sketched in **Fig. 10b**, a lateral spring ($K_{s,l}$) and a lateral dashpot ($C_{s,l}$) are added at the top of the SDOF system, calculated according to Eqs. 10 and 11, respectively.

Finally, System C (**Fig. 10c**) accounts for the true bending stiffness of the deck, replacing the fixity at the top of the SDOF system with a rotational spring ($K_{r,l}$) and a rotation dashpot ($C_{r,l}$). The rotational spring represents the flexural stiffness of the deck, and is computed considering a continuous beam of three equal spans:

$$K_{r,l} = \frac{9\,EI_d}{L_s} \tag{16}$$

where E and I_d : the Young's modulus (RC) and the moment of inertia of the deck, and L_s : the length of each span. For a different number of spans, the equivalent rotational spring

can be computed in exactly the same manner, using similar simple formulas. The rotational dashpot ($C_{r,l}$) is computed as in the previous cases:

$$C_{r,l} = \frac{2\,K_{r,l}\,\xi_s}{\omega} \tag{17}$$

The three simplified models are comparatively assessed in **Fig. 11**. In contrast to the transverse direction, the performance of the simplest System A is not that poor. Thanks to the developing frame action, the stiffness of the bridge in the longitudinal direction is substantially larger ($12EI_p/h^3$ as opposed to $3EI_p/h^3$ for the transverse direction) and the contribution of the abutment bearings is much less pronounced. As depicted in **Fig. 11a**, the pushover capacity predicted by System A is only 12% lower than the capacity of the bridge, as computed using the detailed 3D model. It is interesting to observe that the differences become more pronounced with the increase of the imposed displacement δ. This is simply because the piers unavoidably yield at some point ($\delta \approx 0.04$ m), while the bearings remain elastic for larger displacements. Especially after the piers have consumed their ductility capacity ($\delta > 0.12$ m), the contribution of the (still elastic) abutment bearings becomes more important. Naturally, the assumption of elastic bearing response is a simplification. In reality, the bearings will also yield at some point and their contribution will be limited thereon.

As a result of the above, and in contrast to the transverse direction, the dynamic performance of System A in terms of μ_d/μ_c is acceptable. There is only one case in which System A erroneously predicted collapse, while according to the detailed 3D model μ_d/μ_c had just exceeded 1.2. It is worth observing that the differences are in general more pronounced when the observed (i.e., according to the detailed 3D model) μ_d/μ_c exceeds 1. This is totally consistent with the pushover analysis results, and the previously discussed enhanced contribution of the abutment bearings for larger displacements.

The performance is ameliorated when the abutment bearings are taken into account. As shown in **Fig. 11b**, the pushover capacity predicted by System B is only 3% lower than the capacity of the bridge, as computed using the detailed 3D model. The simplified model compares well with the detailed 3D model in terms of μ_d/μ_c, and there is no erroneous prediction of collapse. Therefore, it may be concluded that the lateral stiffness of the abutment bearings plays a role in the longitudinal direction and should be taken into account. Admittedly, however, their role is not as pronounced as in the transverse direction. The assumption of rotational fixity at the top of the pier also seems to be reasonable.

The effect of the true bending stiffness of the deck can be quantified by examining the performance of System C. As shown in **Fig. 11c**, the static pushover response of System C compares very well with that of the detailed 3D model, especially before yielding of the pier (δ < 0.04 m). For this range of δ, while Systems A and B were stiffer than the detailed 3D model, the F–δ response of System C is a perfect match. Before yielding of the piers, the assumption of full fixity plays a role and introducing the true bending stiffness of the deck leads to substantial improvement. After yielding of the piers, and especially after their ductility capacity is consumed (δ > 0.12 m), the effective stiffness of the pier becomes much lower than that of the deck, rendering the assumption of full rotational fixity a realistic approximation. This also becomes evident when examining the dynamic analysis results: the match between System C and the detailed 3D model is profoundly ameliorated for μ_d/μ_c < 0.5. The mean average percentage error (MAPE) does not exceed 8%, and hence System C is considered as a reasonable approximation.

5. Simplified models accounting for nonlinear SSI

The proposed models (and specifically System C) have been shown to offer a reasonable approximation for both directions of seismic loading (longitudinal and transverse). So far, fixed base conditions have been considered. An extension of System C is proposed in order to account for SSI. Before proceeding to the definition of the simplified model, the effect of the flexibility of the abutments is briefly examined. The full 3D model of the bridge–abutment–foundation–soil system (**Fig. 6c**) is used for this purpose. The latter requires substantial computational effort, calling for careful selection of the seismic excitations. Hence, from the 29 records of **Fig. 7**, three characteristic records are selected: (a) Aegion, which is considered representative of moderate intensity shaking; (b) Lefkada-2003, which contains multiple strong motion cycles and can be considered representative of medium intensity shaking; and (c) the notorious Rinaldi-228 record (Northridge 1994), containing a very strong forward rupture directivity pulse, and being representative of very strong seismic shaking.

Figure 12 illustrates the time histories of deck displacement δ to the response of abutment A1 using the Rinaldi-228 record as seismic excitation in the longitudinal and the transverse direction. It may be concluded that the displacement of the abutment is minor compared to that of the deck. The same conclusion is drawn for all three seismic excitations, and for both directions of loading. Hence, the assumption of fixed base conditions at the abutments can be considered realistic, at least for the purposes of developing adequately simplified models for the purposes of a RARE system. Therefore, it may be considered reasonable to focus on the piers and the additional compliance that is provided by the soil–foundation system.

A simplified method to analyse the seismic performance of foundation–structure systems accounting for nonlinear SSI has been introduced in Anastasopoulos & Kontoroupi [2014]. The latter is extended to the bridge systems studied herein, as schematically illustrated in **Fig. 13a**. The bridge is represented by System C, which has been shown to perform adequately well for both directions of seismic loading. The soil–foundation system is replaced by horizontal, vertical, and rotational springs and dashpots. The horizontal (K_H and C_H) and vertical (K_V and C_V) springs and dashpots are assumed elastic, and can be directly obtained by published solutions [Gazetas, 1983]. This may be considered a reasonable approximation for most bridge piers, the response of which has been shown to be rocking–dominated, provided that $h/B > 1$ [Gajan & Kutter, 2009]. For the rotational degree of freedom, a *nonlinear rotational spring* is employed, accompanied by a *linear dashpot*. The nonlinear rotational spring is defined on the basis of moment–rotation (M–ϑ) relations, computed through displacement–controlled monotonic pushover analyses using a 3D FE model of the soil-foundation system. As discussed in Anastasopoulos & Kontoroupi [2014], the M–ϑ response is divided in three characteristic phases: (i) quasi–elastic response ($\vartheta \rightarrow 0$); (b) plastic response (ultimate state, large ϑ); and (c) nonlinear response (intermediate stage).

The initial *quasi-elastic* rotational stiffness has been shown to be a function of the factor of safety against vertical loading F_S :

$$K_{R,0} = K_{R,elastic}\left(1 - 0.8\frac{1}{F_S}\right) \tag{18}$$

where $K_{R,elastic}$ is the purely elastic rotational stiffness [Gazetas, 1983]:

$$K_{R,elastic} = 3.65\frac{G\,b^3}{1-\nu} \tag{19}$$

in which b is the half width of the footing (= B/2), G is the small strain shear modulus of soil,

and *v* the Poisson's ratio.

The *plastic response* refers to the ultimate capacity of the footing, and can be defined on the basis of published failure envelopes [e.g., Gazetas et al., 2012]:

$$M_u = 0.55\, N_u B \left(1 - \frac{N_u}{N_{uo}}\right) \tag{20}$$

where N_{uo} is the bearing capacity for purely vertical loading [Meyerhof, 1953; Gourvenec, 2007]:

$$N_{uo} \approx (\pi + 3) S_u B^3 \tag{21}$$

Finally, the *nonlinear response* corresponds to the intermediate phase between the quasi-elastic and plastic response. A non-dimensional formulation has been proposed in Anastasopoulos & Kontoroupi [2014], expressing the *M*–ϑ relations in non-dimensional form:

$$M / S_u B^3 = f(\theta / \theta_s) \tag{22}$$

where ϑ_S is a characteristic rotation, defined as follows:

$$\theta_s \approx \frac{N\, B}{4\; K_{R,0}} \tag{23}$$

As shown in **Fig. 13b**, this normalization leads to a single non–dimensional *moment–rotation* curve. The latter is simplified through a piecewise linear approximation, encompassing: (a) a quasi-elastic branch ($\vartheta/\vartheta_s \leq 1/3$); (b) a plastic branch ($\vartheta/\vartheta_s > 10$); and (c) a four-segment intermediate nonlinear branch ($1/3 < \vartheta/\vartheta_s \leq 10$).

As discussed in Anastasopoulos & Kontoroupi [2014], a nonlinear rotational dashpot would ideally be required. However, most FE codes accept a single value of C_R, and hence a simplifying approximation is necessary to maintain simplicity. C_R is assumed to be a function of the effective rotational stiffness K_R, the hysteretic damping ratio ξ, and a characteristic frequency ω:

$$C_R \approx \frac{2\,K_R\,\xi}{\omega} \tag{24}$$

K_R is directly computed from the M–ϑ relations of **Fig. 13b**. The damping ration ξ is computed through the M–ϑ loops of displacement–controlled cyclic pushover analyses, employing the 3D FE model of the soil-foundation system. As shown in **Fig. 13c**, the normalized damping coefficient $C_R/K_{R,elastic}\omega^{-1}$ with respect to ϑ is a "bell shaped" curve, with its maximum at $\vartheta \approx 10^{-3}$ rad (for the studied foundation). As shown in Anastasopoulos & Kontoroupi [2014], the maximum value of the curve can be used as a reasonable simplifying approximation, in order to compute C_R as a function of F_S only.

The efficiency of the proposed simplified model is assessed through comparison with the full 3D model of the bridge–abutment–foundation–soil system (**Fig. 6c**). The comparison is performed in terms of time histories of deck drift δ and moment–curvature (M–c) response of pier P1 (right column). As depicted in **Fig. 14**, the simplified model compares well with the full 3D model when considering the transverse direction of seismic loading. In the case of the moderate intensity Aegion seismic excitation (**Fig. 14a**), the time histories of δ are practically identical, and the comparison is excellent in terms of the maximum value. There is a phase difference after the main pulse, which is consistent with the observed differences in the M–c response. The comparison is equally successful for larger intensity seismic shaking using the Lefkada-2003 record as seismic excitation (**Fig. 14b**). The simplified model slightly under-predicts the response, but the comparison is quite acceptable both in terms of δ and M–c loops. The performance of the simplified model remains satisfactory even for very strong shaking with the Rinaldi-228 record (**Fig. 14c**). The simplified model slightly over-predicts the response in terms of δ, but correctly predicts the exhaustion of ductility capacity of the pier, which enters the descending branch of response.

The comparison is equally successful when considering the longitudinal direction of loading (**Fig. 15**). The comparison is even better for the Aegion seismic excitation (**Fig. 15a**), with the time histories of δ exhibiting exactly the same maximum value and the M–c response being in even better agreement. The same applies to the Lefkada-2003 seismic excitation (**Fig. 15b**), in which case the simplified model nicely captures the time history of δ and the M–c response. The comparison is quite satisfactory for very strong shaking with the Rinaldi-228 record (**Fig. 15c**). As for the transverse direction, the simplified model over-predicts the response in terms of δ, but to a lesser extent. The comparison in terms of M–c loops is considered excellent.

6. Synopsis and conclusions

The paper has developed a simplified method to analyze the seismic performance of typical motorway bridges, accounting for the contribution of the key structural components (deck and abutment bearings) and nonlinear soil–structure interaction (SSI). For this purpose, a typical overpass bridge of the Attiki Odos Motorway in Athens (Greece) is used as an illustrative example. Besides its simplicity, the selected system is representative of about 30% of the bridges of Attiki Odos, and is also considered rather common for metropolitan motorways in general. Attiki Odos is used as a case study for a RApid REsponse (RARE) system that is currently being developed, and is therefore of particular interest. The development of such a RARE system requires analysis of the seismic performance of a very large number of bridges subjected to a variety of seismic excitation scenarios. Conducting such analysis with full 3D models of the bridge–abutment–foundation–soil system would require substantial computational effort, rendering the use of simplified models a practical necessity.

The seismic performance of the bridge has been analyzed employing the FE method. Two models were developed for this purpose: a detailed 3D model of the bridge assuming fixed base conditions; and a full 3D model of the bridge–abutment–foundation–soil system. The first model incorporated the piers, accounting for their nonlinear response, the deck, and the abutment bearings. In the latter case, all material (superstructure and soil) and geometric (uplifting and sliding) nonlinearities were accounted for. The detailed models of the bridge were used as reference to assess the efficiency of the simplified method. Initially, SSI was ignored to focus on the effect of key structural components of the bridge (deck and abutment bearings). Then, the simplified models were extended to account for SSI.

The proposed simplified model for fixed base conditions (System C, **Figs. 8** and **10**) is composed of an equivalent SDOF system of a single bridge pier, with lateral and rotational springs and dashpots connected at the top, representing the deck and the abutment bearings. As summarized in the flowchart of **Fig. 16**, the definition of the simplified model requires section analysis of the most vulnerable pier, and computation of spring and dashpot coefficients using simple formulas. Comparing three simplified models of varying complexity, it is shown that the contribution of the lateral and rotational restraint provided by the deck and the system of abutment bearings is not at all negligible and should be taken into account. The proposed simplified model compares well with the detailed 3D model of the bridge, both in terms of static pushover response and with respect to the dynamic time history analyses. It is therefore considered a reasonable approximation of the actual response of the bridge, and can be particularly useful in the context of a RARE system.

The simplified models were further extended to account for nonlinear SSI. The full 3D model of the bridge–abutment–foundation–soil system was used as a benchmark in this case. Initial analyses showed that the displacement of the abutments is minor compared to

that of the deck, and therefore it is reasonable to focus on the foundations of the piers. A simplified method to analyse the seismic performance of foundation–structure systems accounting for nonlinear SSI has been introduced in Anastasopoulos & Kontoroupi [2014], and is currently extended to the bridge systems studied herein (**Fig. 13**). The soil–foundation system is replaced by horizontal, vertical, and rotational springs and dashpots. The horizontal (K_H and C_H) and vertical (K_V and C_V) springs and dashpots are assumed elastic (see also **Fig.16**). The nonlinear rotational spring is defined on the basis of moment–rotation (M–ϑ) relations, computed through displacement–controlled monotonic pushover analyses using a 3D FE model of the soil–foundation system. In terms of a simplifying approximation, the rotational dashpot C_R is assumed elastic, being a function of the effective rotational stiffness K_R, the hysteretic damping ratio ξ, and a characteristic frequency ω. The simplified model is shown to compare well with the full 3D model of the bridge–abutment–foundation–soil system.

Although the proposed simplified models are based on several simplifying approximations, they are considered reasonably accurate especially in the context of developing a RARE system for metropolitan motorways. Despite the fact that the paper focused on a representative but specific bridge system, the results are considered of more general validity. The same methodology can be employed to derive similar simplified models for different bridge classes and/or different foundation types.

Acknowledgement

The financial support for this paper has been provided by the research project "SYNERGY 2011" (Development of Earthquake Rapid Response System for Metropolitan Motorways) of GGET–EYDE–ETAK, implemented under the "EPAN II Competitiveness & Entrepreneurship", co-funded by the European Social Fund (ESF) and national resources.

References

ABAQUS 6.11. (2011). Standard user's manual. Dassault Systèmes Simulia Corp., Providence, RI, USA.

Agalianos A., Sakellariadis L. (2013). *A simplified method to estimate seismic vulnerability of bridges considering soil-structure interaction.* Diploma Thesis, National Technical of Athens, Greece.

Anastasopoulos I., Gelagoti F., Kourkoulis R., Gazetas G. (2011), "Simplified Constitutive model for Simulation of Cyclic Response of Shallow Foundations: Validation against Laboratory Tests", *Journal of Geotechnical and Geoenvironmental Engineering*, ASCE, 137(12), pp. 1154–1168.

Anastasopoulos I., Kontoroupi Th. (2014), "Simplified approximate method for analysis of rocking systems accounting for soil inelasticity and foundation uplifting", *Soil Dynamics and Earthquake Engineering*, Vol. 56, pp. 28-43.

Anastasopoulos I., Anastasopoulos P.Ch., Agalianos A., and Sakellariadis L. (2014), "Simple method for real–time seismic damage assessment of bridges", *Soil Dynamics and Earthquake Engineering* (submitted for possible publication).

Arias A. (1970). "A measure of earthquake intensity", In: Hansen RJ (ed) *Seismic design for nuclear power plants*. MIT Press, Cambridge, pp 438–483.

Argyroudis S., Monge O., Finazzi D., Pessina V. (2003). *Vulnerability assessment of lifelines and essential facilities: methodological handbook*, Appendix 1: Roadway transportation system. Report n°GTR-RSK 0101-152av7.

ATC-13 (1985). —Earthquake damage evaluation data for California. Redwood City, California.

EAK (2000) "Greek Seismic Code", Organization of Seismic Planning and Protection, Athens (in Greek).

ΕΚΩΣ (2000) "Greek code for reinforced concrete", Organization of Seismic Planning and Protection, Athens (in Greek).

Codermatz R., Nicolich R., Slejko D. (2003). "Seismic risk assessments and GIS technology: applications to infrastructures in the Friuli-Venezia Giulia region (NE Italy)". *Earthquake Engineering and Structural Dynamics,* Vol.32, pp. 1677-1690.

De Groeve T., Vernaccini L., Annunziato A. (2006). Global Disaster Alert and Coordination System, *Proc. 3rd International ISCRAM Conference*, Eds. B. Van de Walle and M. Turoff, Newark, pp.1-10.

Erdik M., Fahjan Y., Ozel O., Alcık H., Mert A., Gul M. (2003) "Istanbul earthquake rapid response and early warning system," Bulletin of Earthquake Engineering, 1(1) 157–63.

Erdik M., Sesetyan K., Demircioglu M.B., Hancilar U., Zulfikar C. (2011). "Rapid earthquake loss assessment after damaging earthquakes," Soil Dynamics and Earthquake Engineering, 31, 247–266.

FHWA [Federal Highway Administration] (1995) Recording and coding guide for the structure inventory and appraisal of the nation's bridges. Rep. no. FHWA-PD-96-001, Office of Engineering, Bridge Division, Washington, DC

Franchin P., Pinto P.E. (2009). "Allowing Traffic over Mainshock-damaged Bridges", *Journal*

of Earthquake Engineering, 13(5): 585-599.

Gajan S., Kutter BL. (2009), "Effects of Moment-to-Shear Ratio on Combined Cyclic Load-Displacement Behavior of Shallow Foundations from Centrifuge Experiments" *Journal of Geotechnical and Geoenvironmental Engineering*, ASCE 135(8), pp. 1044-1055.

Gazetas G. (1983), "Analysis of machine foundation vibrations: state of the art", *Soil Dynamics and Earthquake Engineering*, 2, pp. 2–42.

Gazetas G., Anastasopoulos I., Adamidis O., Kontoroupi T. (2012), "Nonlinear Rocking Stiffness of Foundations", *Soil Dynamics and Earthquake Engineering*, 47, pp. 83–91.

Garini E., Gazetas G. (2013). "Damage potential of near-fault records: sliding displacement against conventional "Intensity Measures"". Bull Earthquake Eng (2013) 11:455–480.

Gerolymos N., Gazetas G. (2005), "Seismic Response of Yielding Pile in Non - Linear Soil", Proceedings of the 1 st Greece - Japan Workshop on Seismic Design, Observation, Retrofit of Foundations, Athens, Greece, p.p. 25–37.

Gourvenec S. (2007), "Shape effects on the capacity of rectangular footings under general loading", *Géotechnique*, 57(8), pp. 637-646.

Housner G.W. (1952). "Spectrum intensities of strong motion earthquakes". Proceedings of the Symposium on earthquake and blast effects on structures, EERI, Oakland California, pp. 20–36.

Meyerhof G.G. (1953), "The bearing capacity of foundations under eccentric and inclined loads", *3rd International Conference of Soil Mechanics and Foundation Engineering*, Zurich, 1, 440–445.

Kawashima K., Unjoh S. (1997). "The damage of highway bridges in the 1995 Hyogo-ken Nanbu earthquake and its impact on Japanese seismic design". *Journal of Earthquake Engineering*, 1(3): 505-541.

Koh C.G., and Kelly J.M. (1988). “A simple mechanical model for elastomeric bearings used in base isolation”. *International Journal of Mechanical Sciences*, 30(12): 933-943.

Moschonas I.F., Kappos A.J., Panetsos P., Papadopoulos V., Makarios T., Thanopoulos P. (2009), “Seismic fragility curves for greek bridges: methodology and case studies”, *Bulletin of Earthquake Engineering*, Vol. 7, pp. 439–468.

National Institute of Building Sciences (NIBS) (1999, 2004). —HAZUS: Users’ Manual and Technical Manuals‖. Report prepared for the Federal Emergency Management Agency, Washington, D.C.

Nielson B. & DesRoches R. (2007). “Analytical Seismic Fragility Curves for Typical Bridges in the Central and Southeastern United States,” *Earthquake Spectra*, Volume 23, No. 3, pages 615–633

Pitilakis K., Crowley H. (2014). Recommendations for Future Directions in Fragility Function Research, *Geotechnical, Geological and Earthquake Engineering*, 27, pp. 403-413.

Pitilakis K., Crowley E., Kaynia A. (eds) (2014). *SYNER-G: Typology definition and fragility functions for physical elements at seismic risk*, ISBN 978-94-007-7872-6, Springer Science and Business Media.

Priestley MJN, Seible F, Calvi GM (1996) Seismic design and retrofit of bridges. Wiley, New York.

USC-RC (2001). “Moment-Curvature, Force-Deflection, and Axial Force-Bending Moment Interaction Analysis of Reinforced Concrete Members”. University of S. California, USA.

Von Thun J.L., Rochim L.H., Scott G.A., Wilson J.A. (1988). “Earthquake ground motions for design and analysis of dams”. *Earthquake engineering and soil dynamics II—recent advances in ground-motion evaluation*. Geotechnical Special Publication 20, ASCE, pp 463–481.

Table 1. Classification of Attiki Odos motorway bridges.

Number of spans	Type of deck	Pier-to-deck connection	Description	Code name	Number of cases	Percentage (%)
Single span	Continuous	Fixed	Frame	FR	52	26.9
Single span	Simply Supported	Bearings	Single Span Simply Supported	SSSS	9	4.7
Multi span	Continuous	Fixed	Multi Span Continuous Fixed	MSCF	41	21.2
Multi span	Continuous	Bearings	Multi Span Continuous Bearings	MSCB	11	5.7
Multi span	Continuous	Fixed/ Bearings	Multi Span Continuous Fixed/Bearings	MSCF/B	58	30.1
Multi span	Simply Supported	Bearings	Multi Span Simply Supported	MSSS	1	0.5
Varies	Varies	Varies	Motorway Junctions	MJ	21	10.9

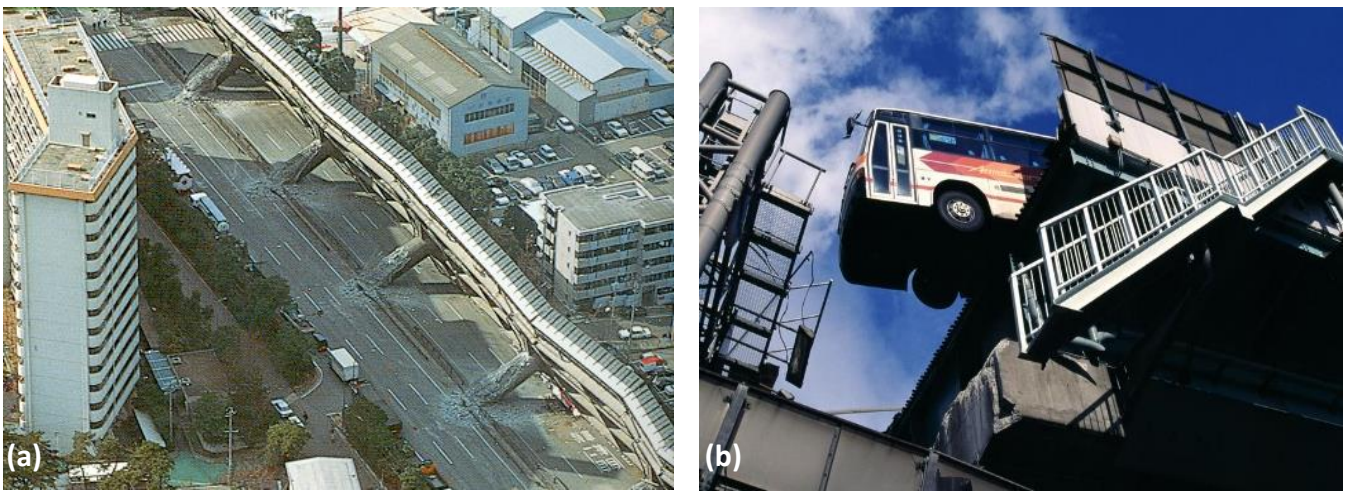

Figure 1. Direct and indirect consequences of an earthquake: (a) collapse of the Fukae section of Hanshin Expressway Route No. 3 during the 1995 Kobe earthquake; and (b) bus stopping just before a collapsed bridge span.

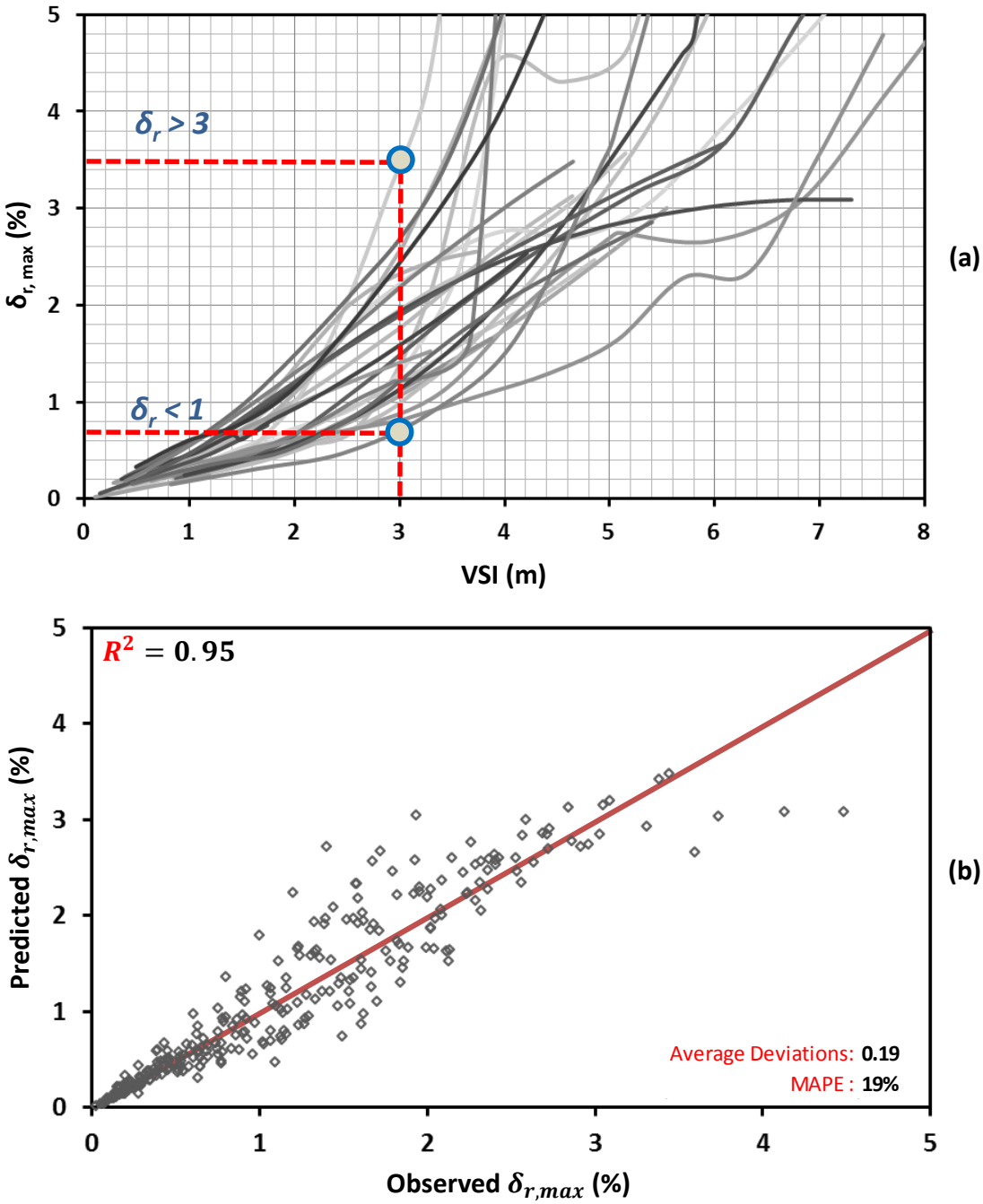

Figure 2. Seismic performance of an idealized bridge pier [Anastasopoulos et al., 2014]: (a) correlation of typical DI (maximum drift ratio $\delta_{r,max}$) with one of the best IMs (VSI); and (b) observed vs. predicted $\delta_{r,max}$ using the nonlinear regression model equation.

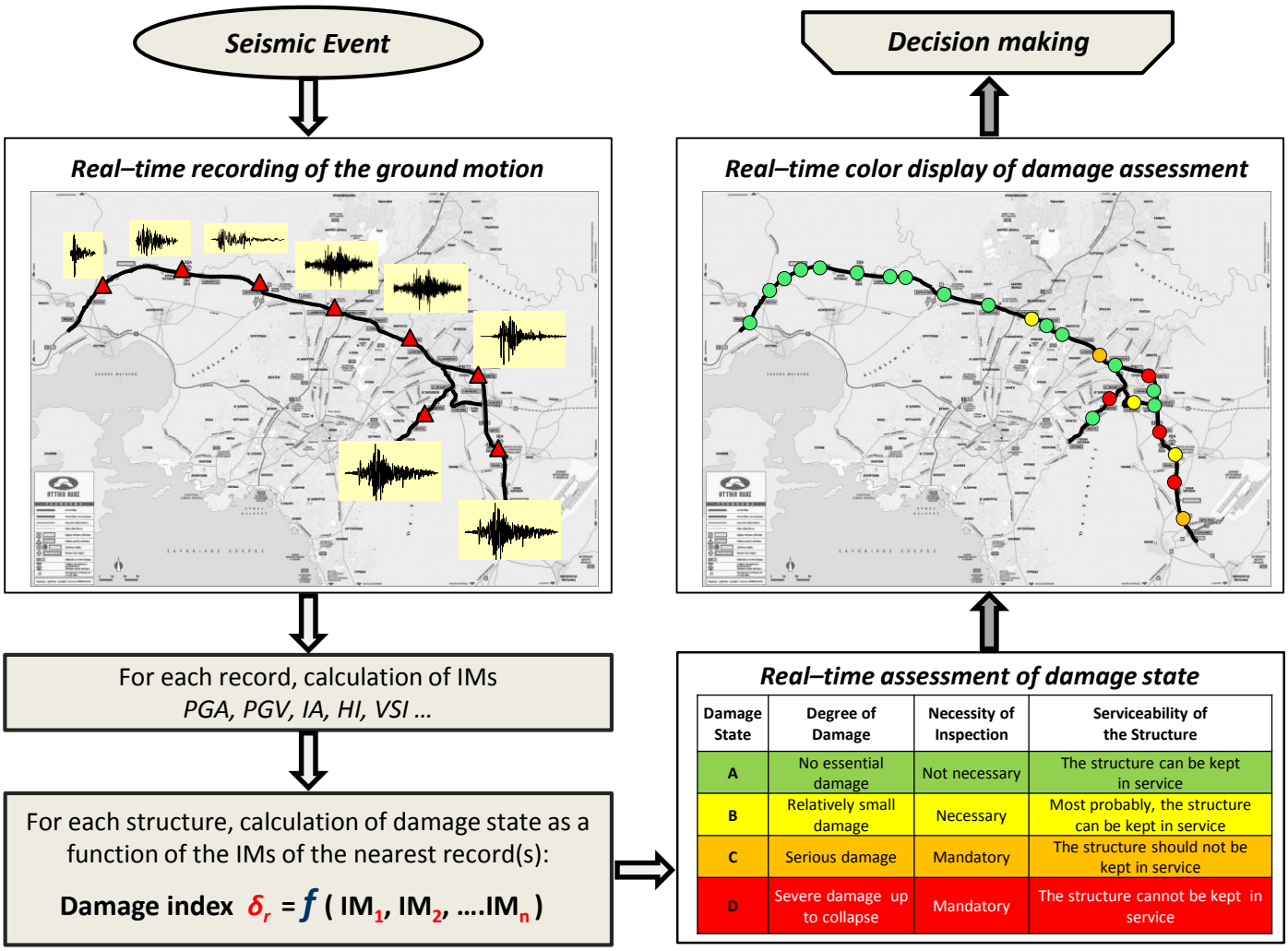

Figure 3. Schematic illustration of the application of the RARE system during a seismic event [Anastasopoulos et al., 2014].

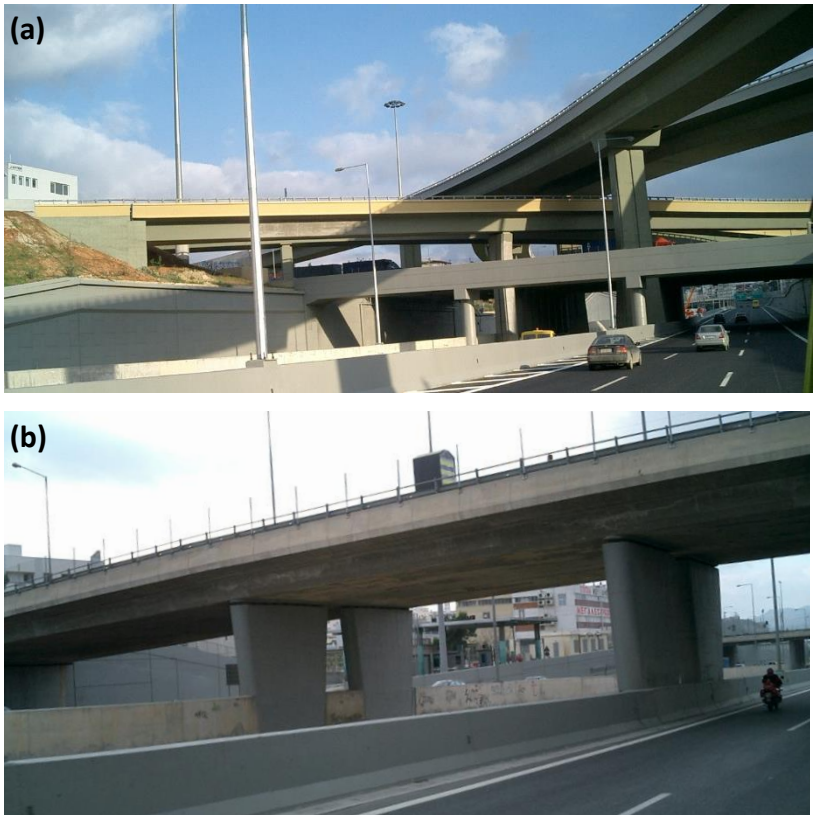

Figure 4. Attiki Odos motorway bridges: (a) example of an interchange; and (b) typical overpass bridge.

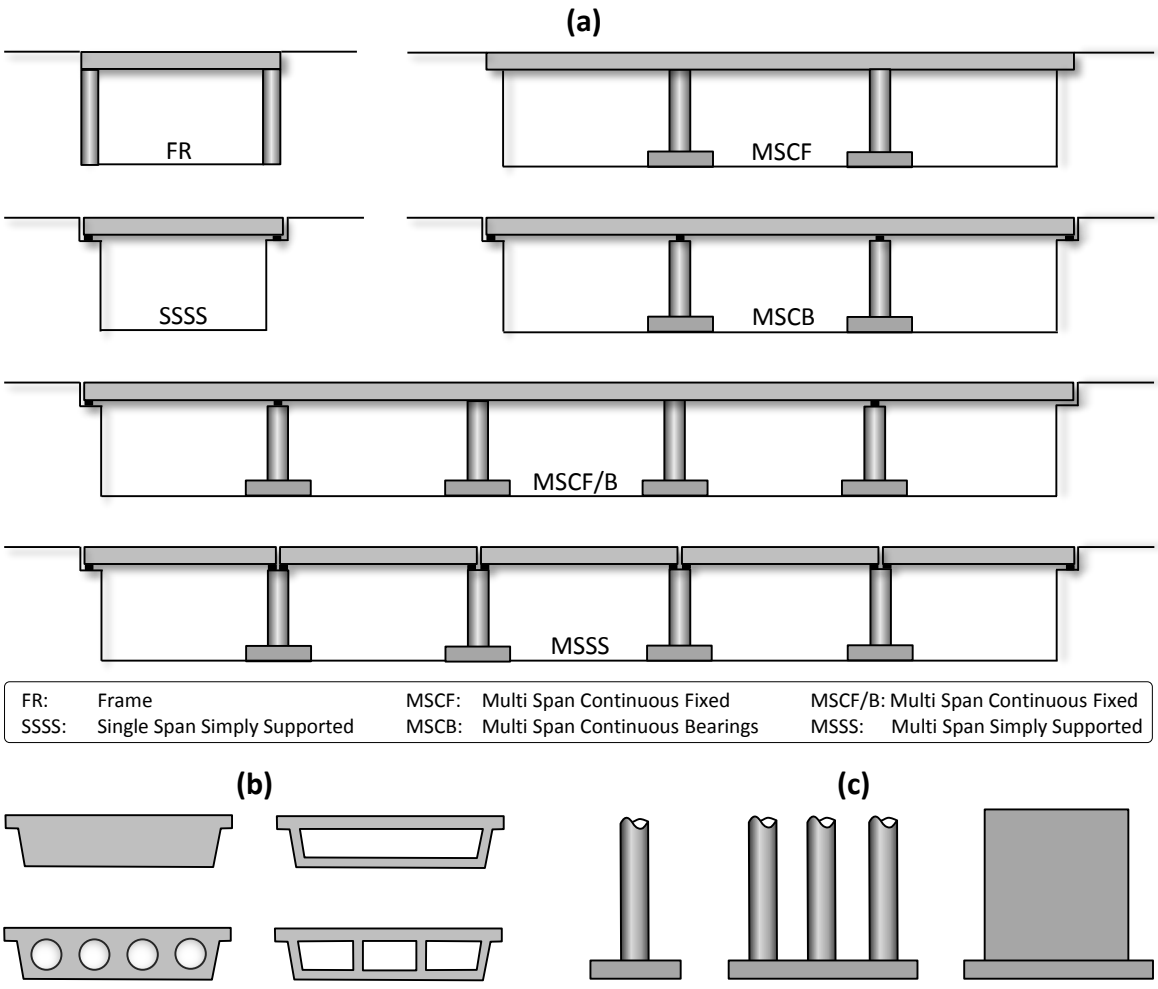

Figure 5. Classification of Attiki Odos bridges: (a) structural typologies; (b) typical deck sections; and (c) typical pier typologies.

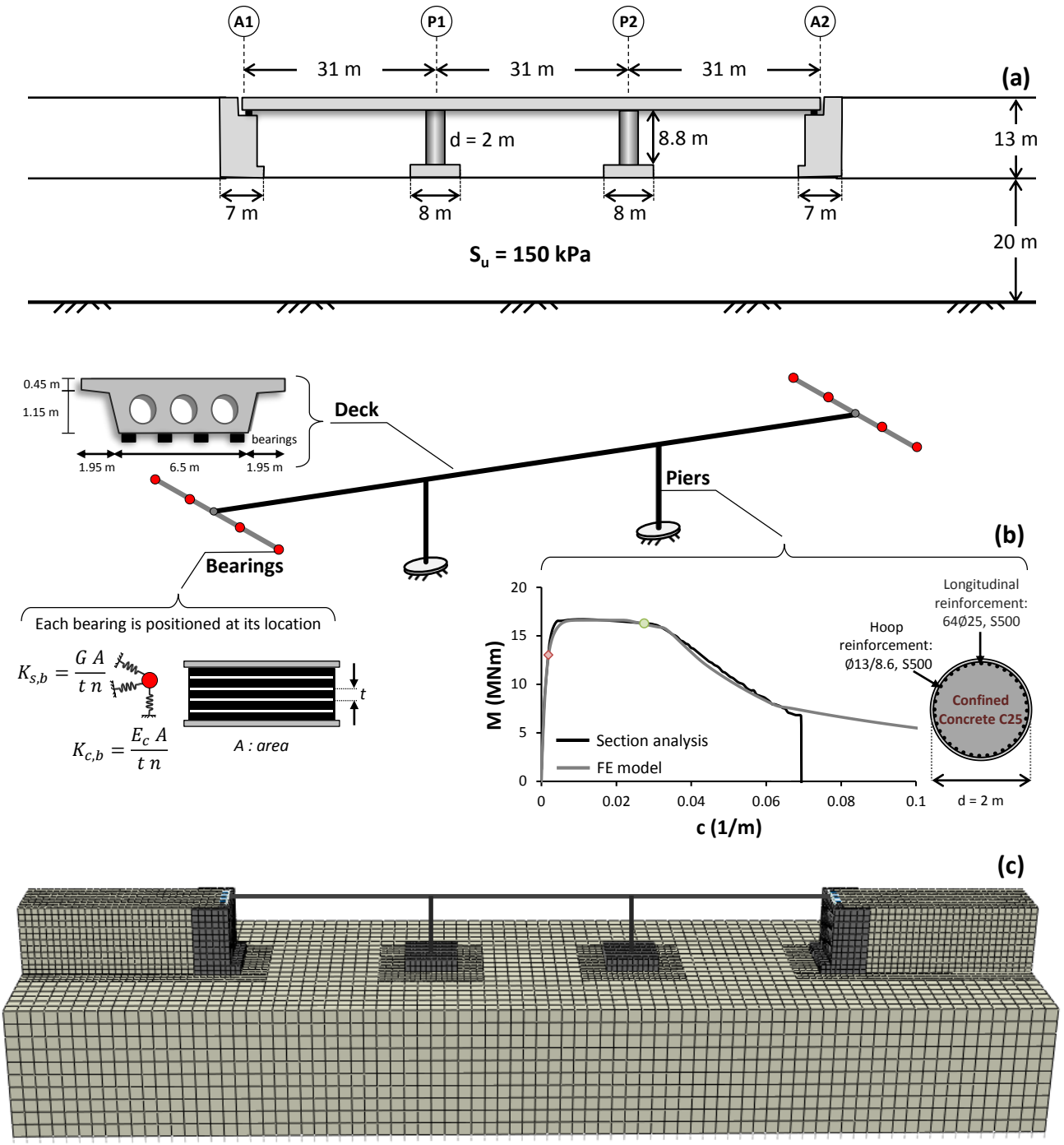

Figure 6. Typical overpass bridge (A01-TE20) of the Attiki Odos motorway used as an example for the analyses: (a) key attributes of the bridge; (b) model assuming fixed base conditions; and (c) full 3D model of the bridge, including the foundations, the abutments, and the subsoil.

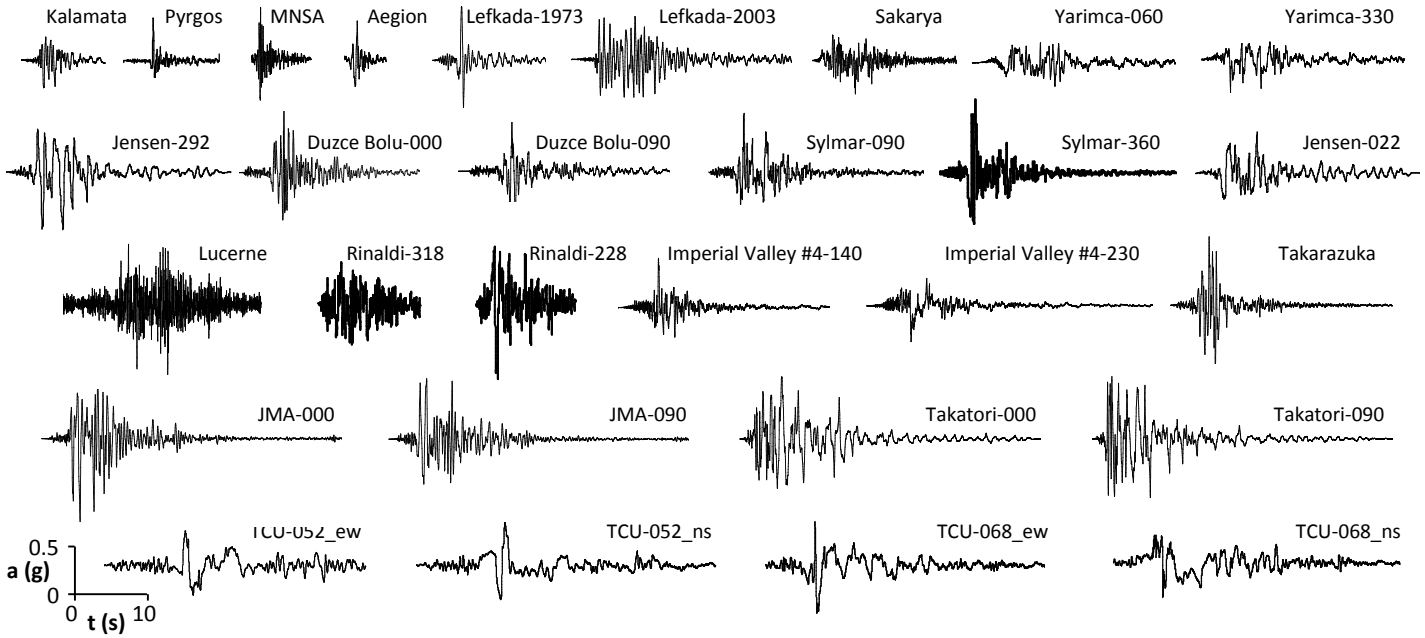

Figure 7. Real records used for the analyses, covering a wide range of seismic excitation characteristics.

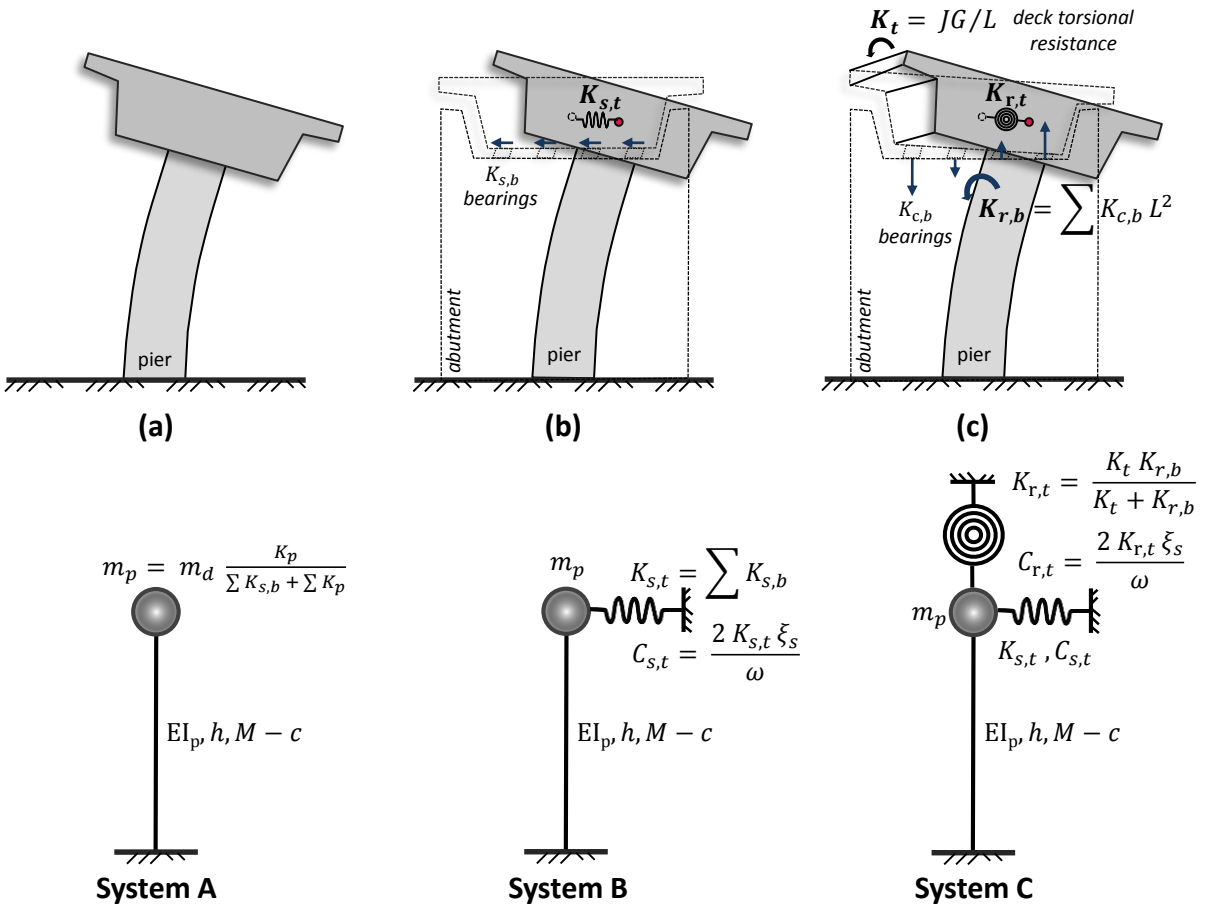

Figure 8. Simplified models assuming fixed–base conditions, for the transverse direction: (a) System A, considering a single pier; (b) System B, taking account of the contribution of the lateral stiffness of the abutment bearings; and (c) System C, also accounting for the rotational restraint provided by the torsional resistance of the deck acting in series with the transverse moment resistance provided by the system of bearings.

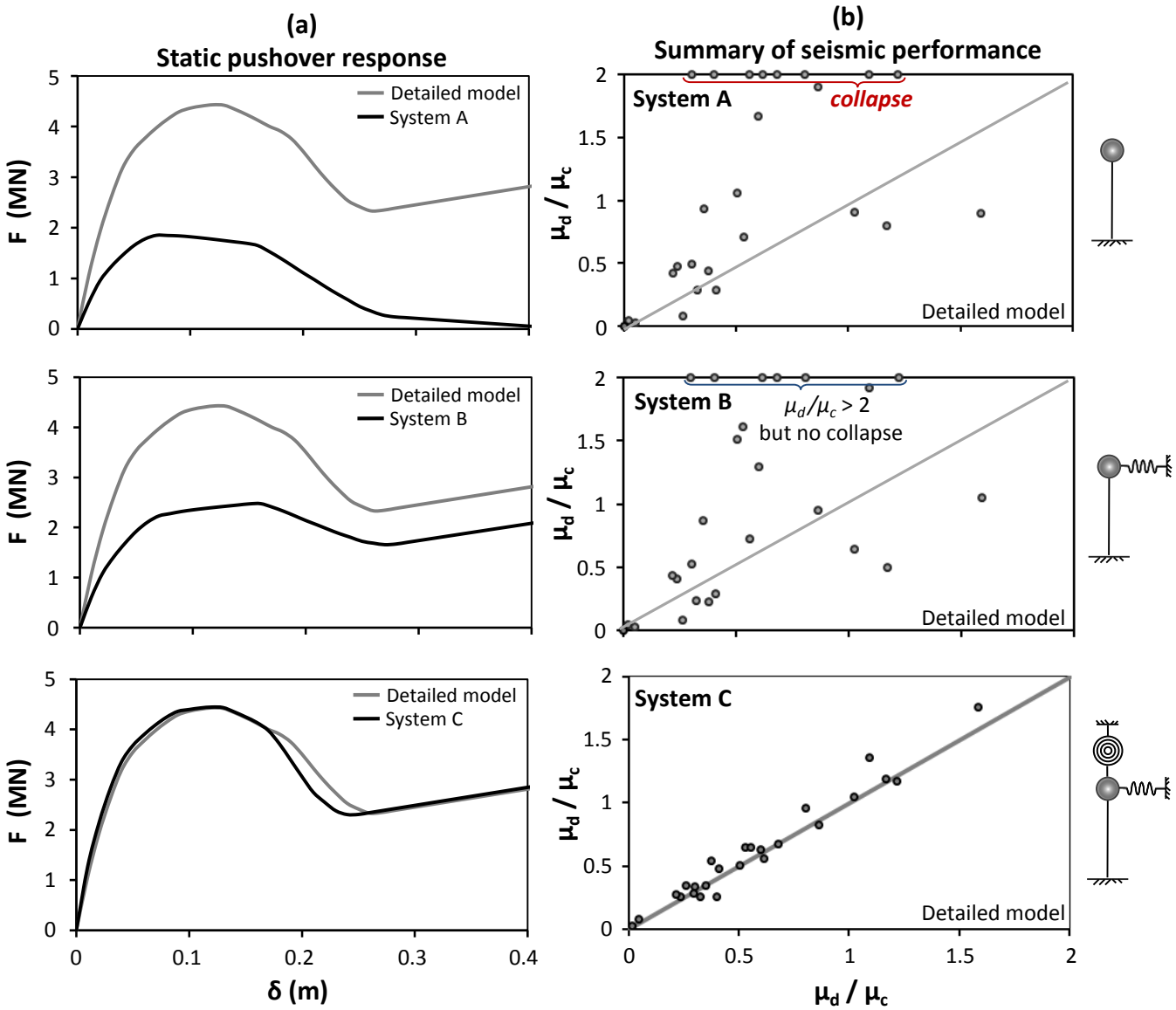

Figure 9. Comparison of the simplified models to the detailed 3D model of the bridge assuming fixed-base conditions–transverse direction: (a) static pushover (F–δ) response; and (b) summary of dynamic time history analyses for all seismic excitations–predicted (simplified models) vs. observed (detailed 3D model) ratio of ductility demand over ductility capacity (μ_d/μ_c).

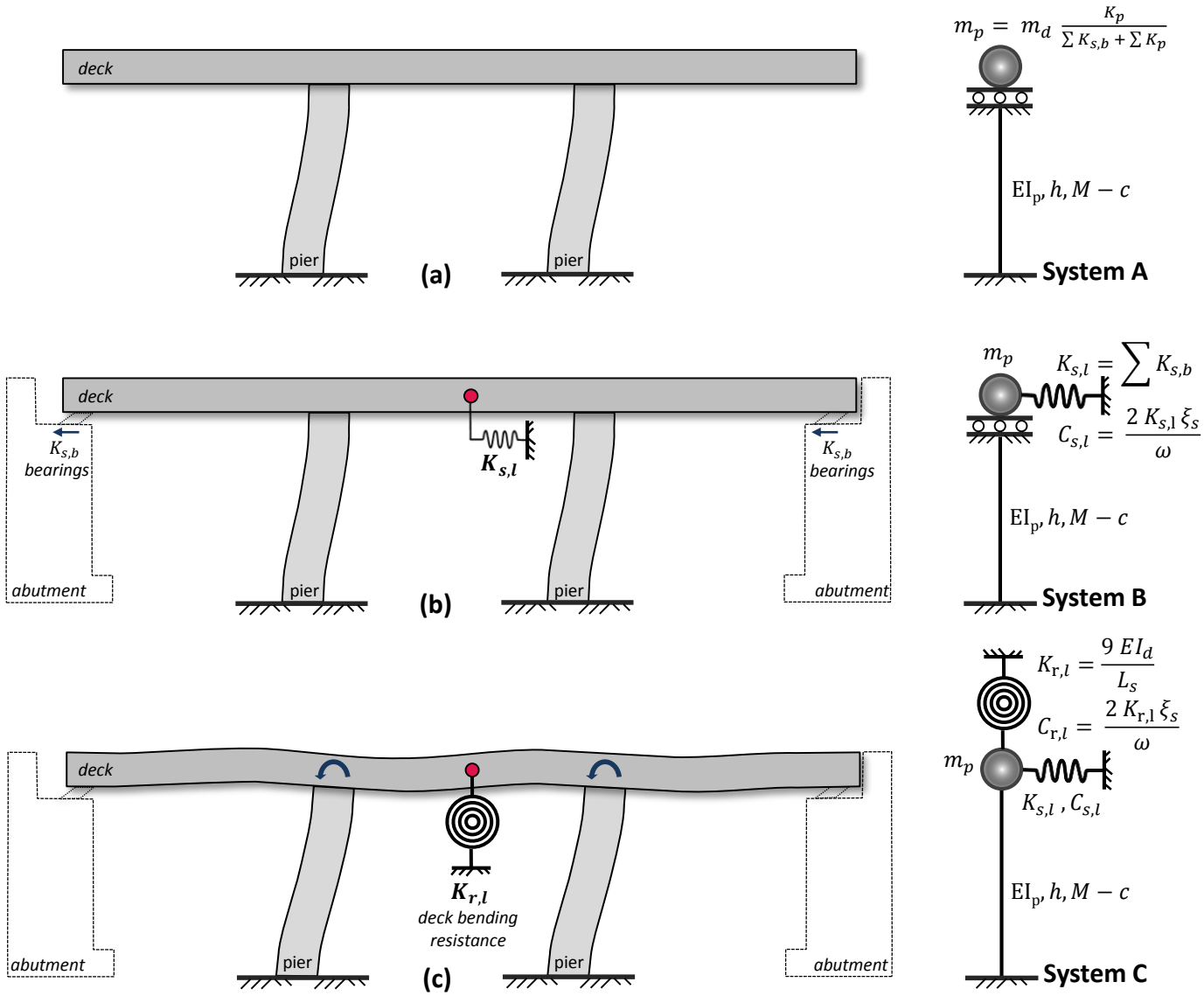

Figure 10. Simplified models assuming fixed–base conditions, for the longitudinal direction: (a) System A, considering a single pier with rotational fixity at the top; (b) System B, taking account of the contribution of the lateral stiffness of abutment bearings; and (c) System C, accounting for the true bending stiffness of the deck, replacing the rotational fixity with a rotation spring and a rotational dashpot.

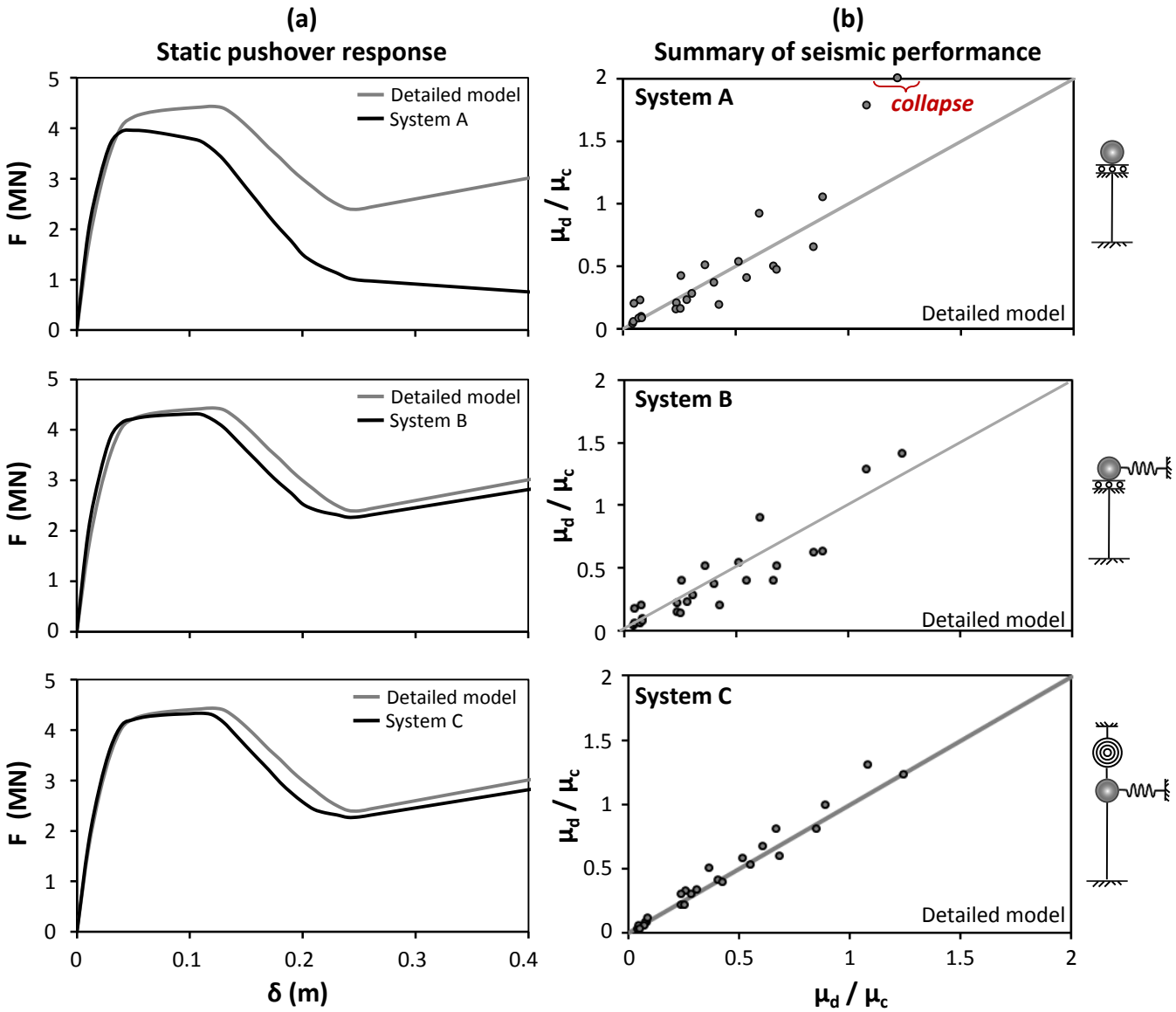

Figure 11. Comparison of the simplified models to the detailed 3D model of the bridge assuming fixed-base conditions–longitudinal direction: (a) static pushover (F–δ) response; and (b) summary of dynamic time history analyses for all seismic excitations–predicted (simplified models) vs. observed (detailed 3D model) ratio of ductility demand over ductility capacity (μ_d/μ_c).

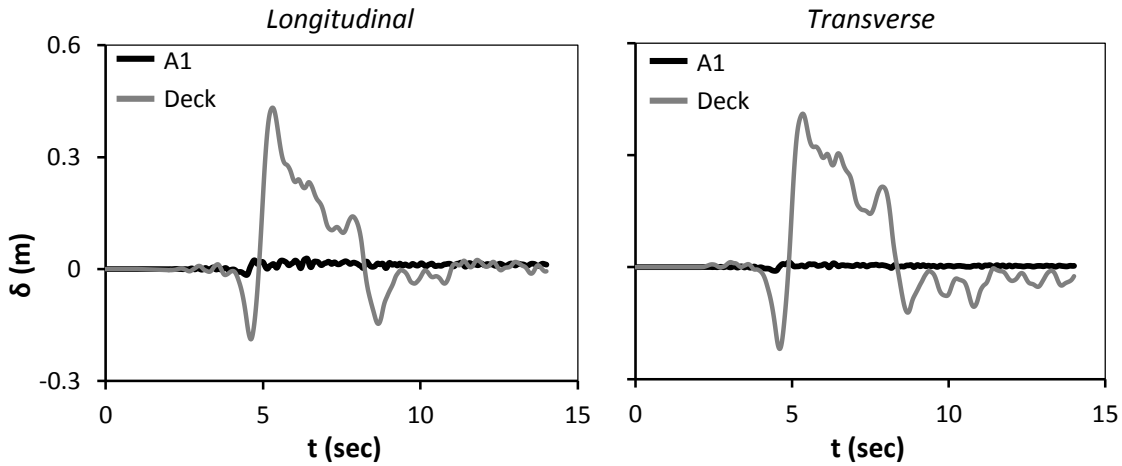

Figure 12. Dynamic time history analysis using the full 3D model of the bridge–foundation–abutment–subsoil system, using the Rinaldi-228 record as seismic excitation in the longitudinal and the transverse direction: time histories of deck displacement δ and comparison to the response of abutment A1.

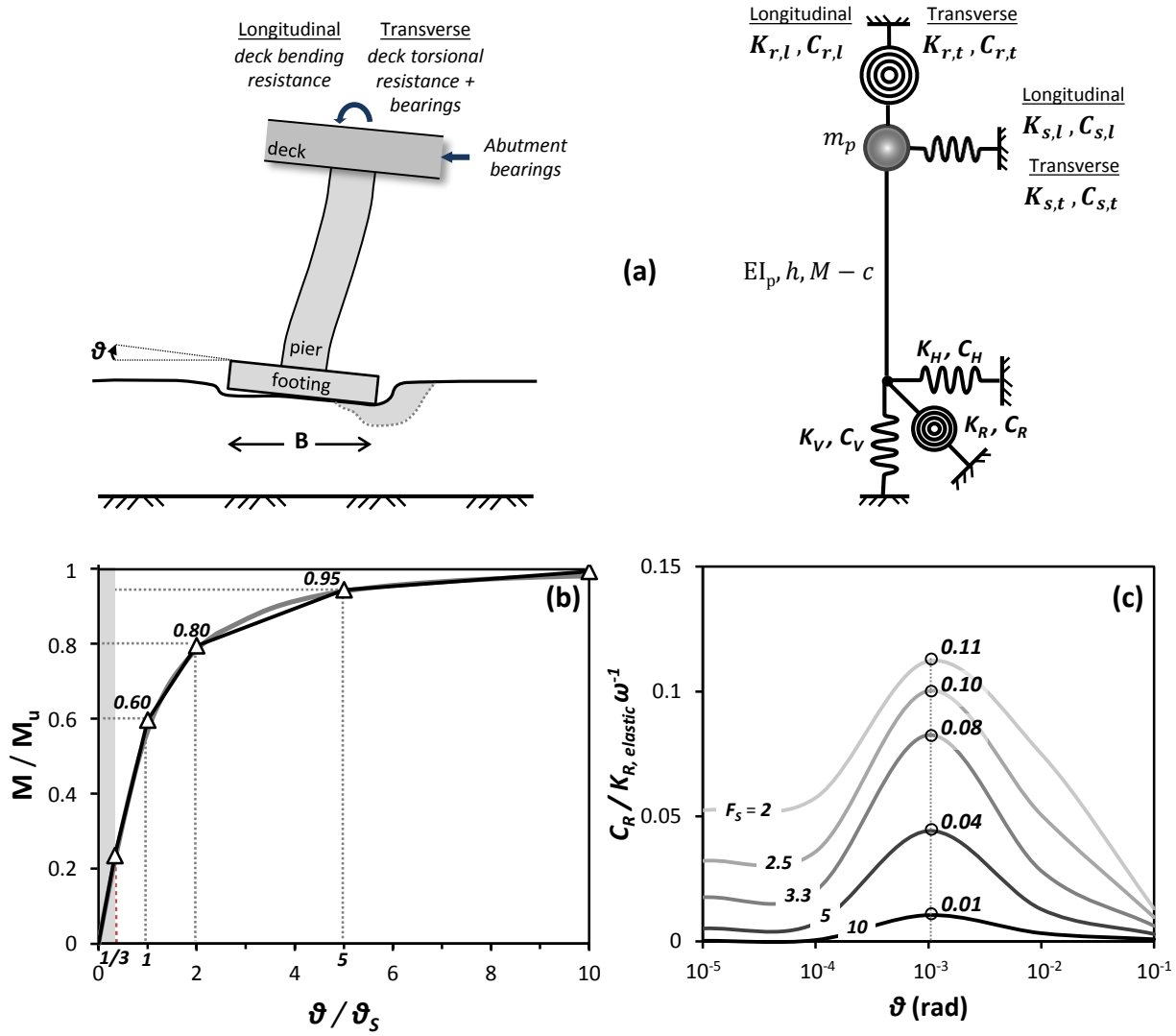

Figure 13. Simplified model accounting for nonlinear SSI: (a) outline of the model, where the soil–foundation system is replaced by a *nonlinear* rotational spring K_R and a linear dashpot C_R , accompanied by linear springs and dashpots in the horizontal (K_H , C_H) and vertical (K_V , C_V) direction; (b) definition of K_R with non-dimensional moment–rotation (M–ϑ) relation and simplified piecewise approximation; and (c) dimensionless damping coefficient $C_R/K_{R,elastic}\omega^{-1}$ with respect to ϑ and F_s [Anastasopoulos & Kontoroupi, 2014].

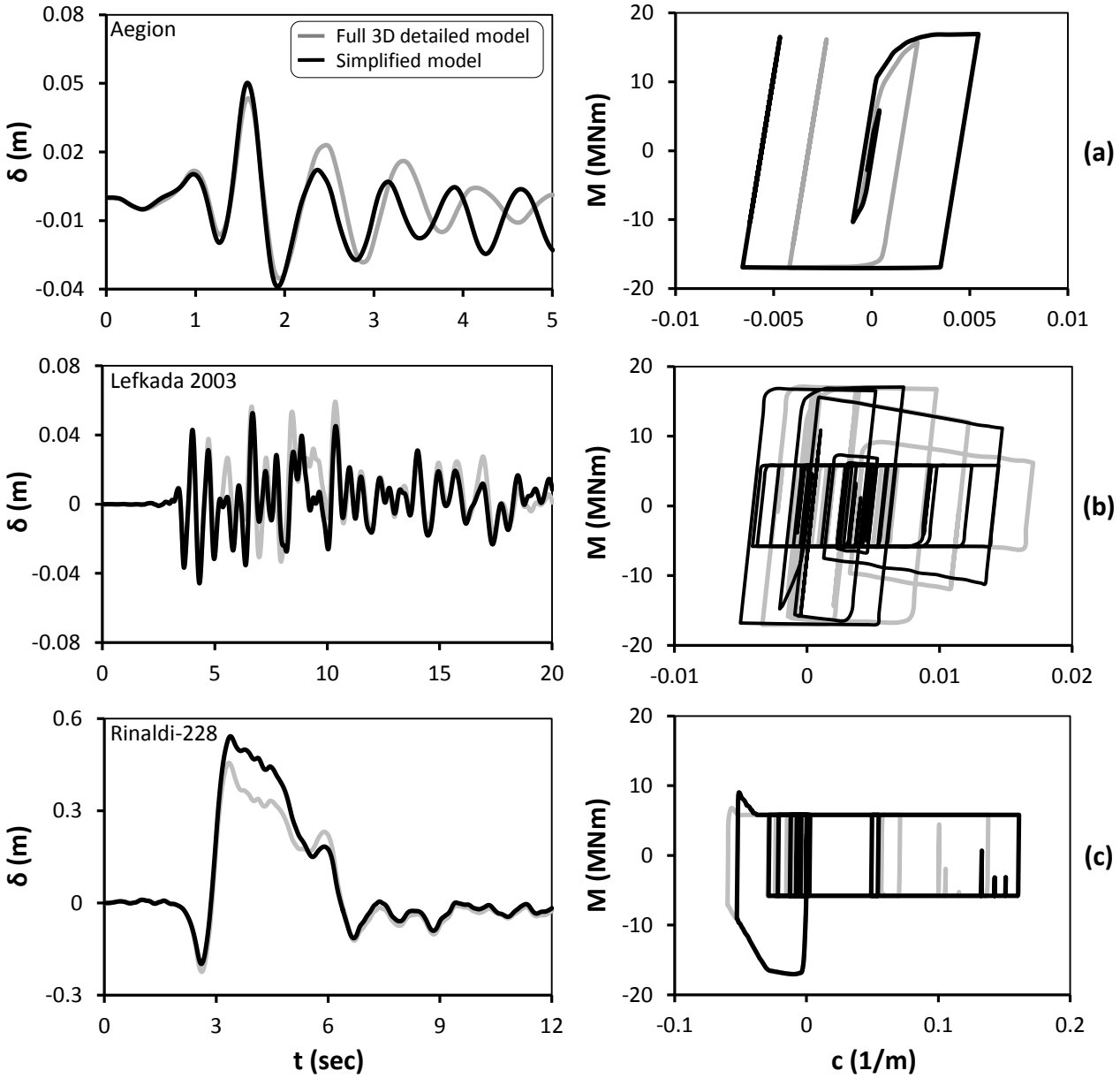

Figure 14. Comparison of the simplified model accounting for SSI to the full 3D detailed model in the transverse direction. Time histories of deck drift δ (left column) and moment–curvature response of pier P1 (right column), using as seismic excitation: (a) Aegion; (b) Lefkada-2003; and (c) Rinaldi-228.

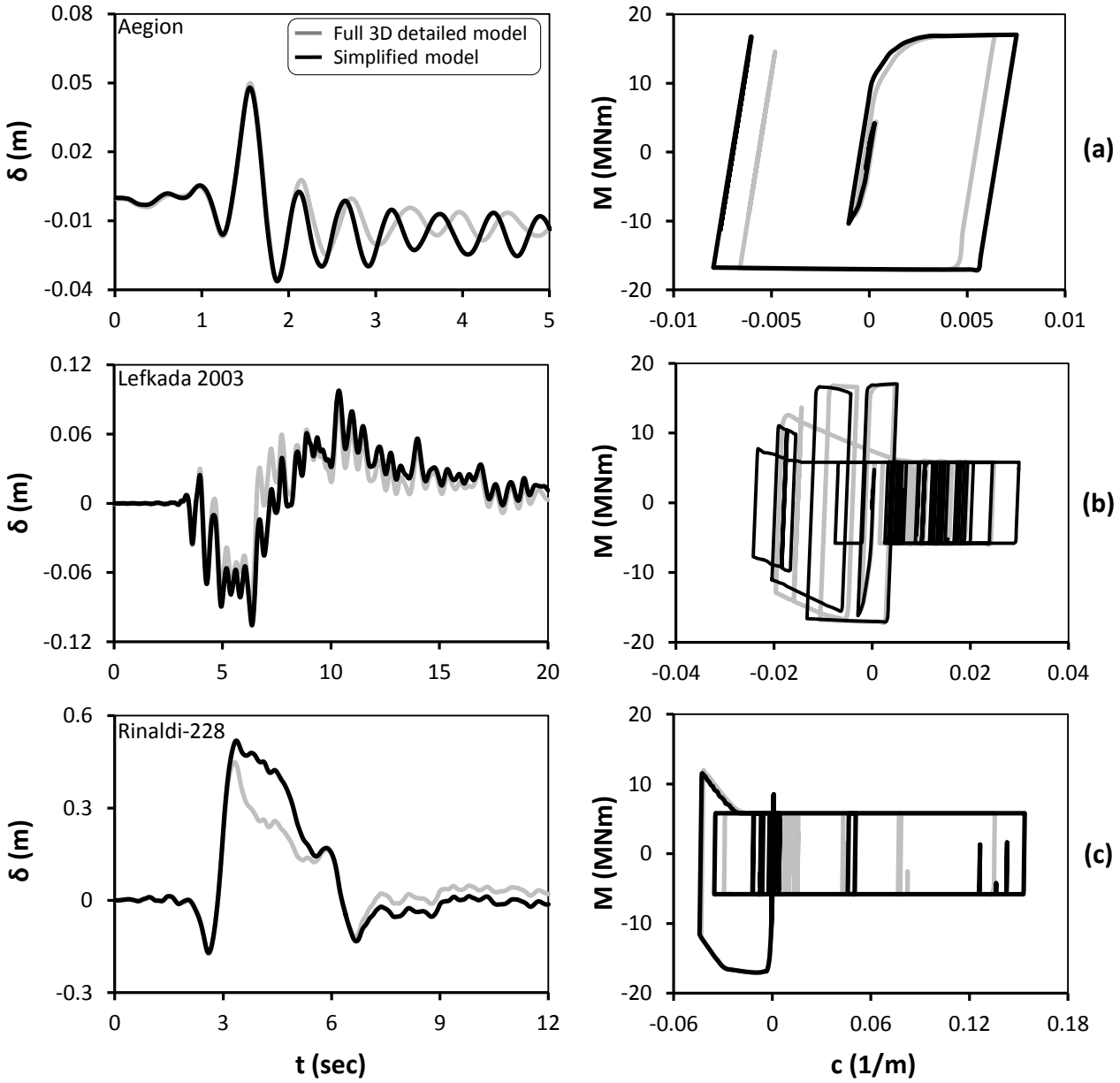

Figure 15. Comparison of the simplified model accounting for SSI to the full 3D detailed model in the longitudinal direction. Time histories of deck drift δ (left column) and moment–curvature response of pier P1 (right column), using as seismic excitation: (a) Aegion; (b) Lefkada-2003; and (c) Rinaldi-228.

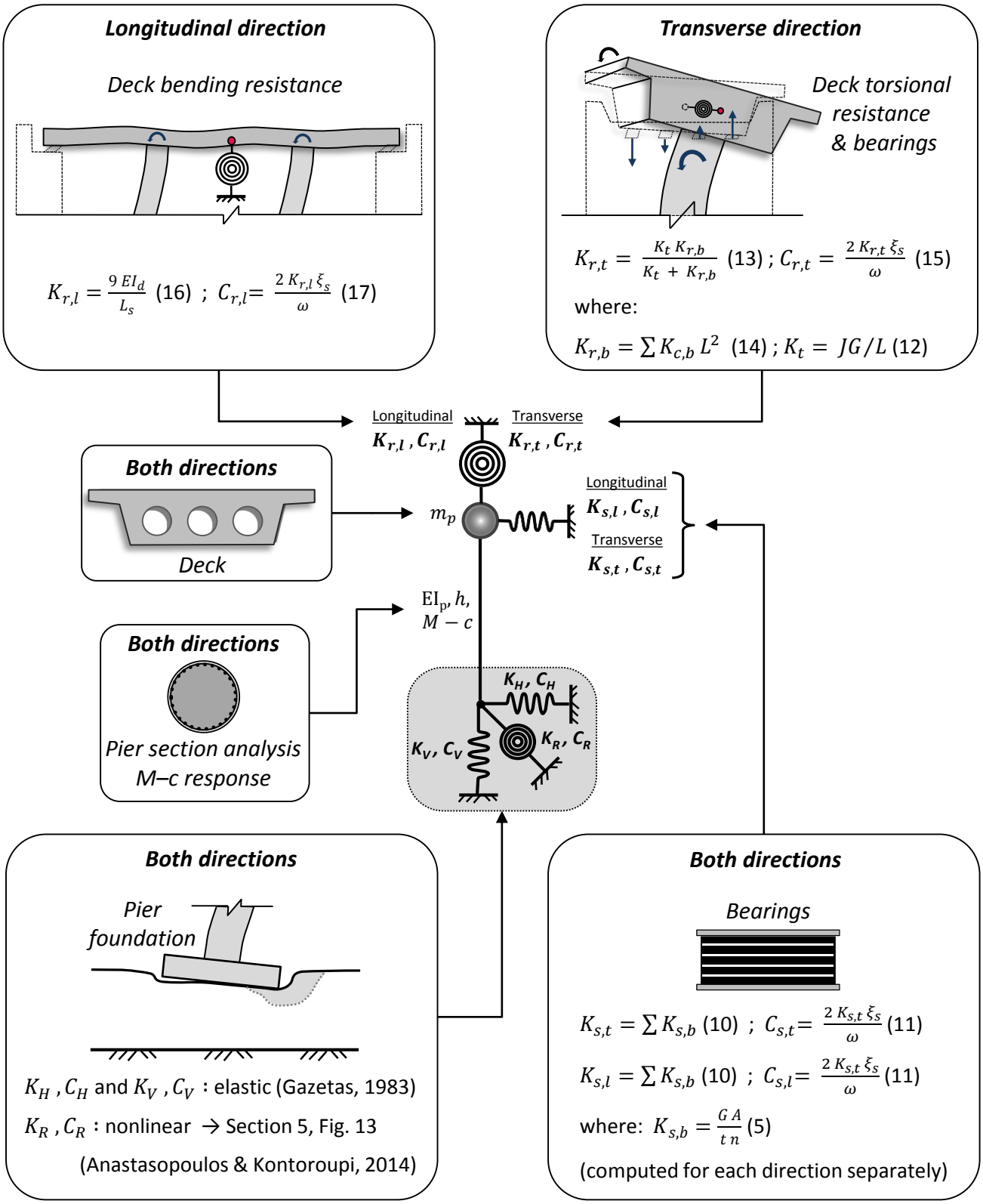

Figure 16. Flowchart summarizing the procedure that is required to set up the simplified model of the bridge, accounting for key structural components and nonlinear soil–structure interaction.